Published in final edited form as:
J Org Chem. 2009 January 2; 74(1): 339–350. doi:10.1021/jo8018945.

Discovery of a sensitive, selective, and tight binding fluorogenic substrate of bovine plasma amine oxidase

Ke-Qing Ling* and **Lawrence M. Sayre***
Department of Chemistry, Case Western Reserve University, Cleveland, OH 44106

Abstract

We report a novel fluorogenic substrate of bovine plasma amine oxidase (BPAO), namely (2-(6-(aminomethyl)naphthalen-2-yloxy)ethyl)trimethylammonium (ANETA), which displays extremely tight binding to BPAO (K_m 183±14 nM), and yet is metabolized fairly quickly (k_{cat} 0.690±0.010 s^{-1}), with the aldehyde turnover product (2-(6-formylnaphthalen-2-yloxy)ethyl)trimethylammonium serving as a real time reporting fluorophore of the enzyme activity. This allowed for the development of a fluorometric non-coupled assay that is two orders of magnitude more sensitive than the spectrophotometric benzylamine assay. The discovery of ANETA involved elaboration of the lead compound 6-methoxy-2-naphthalenemethaneamine by structure-based design, which recognized the ancillary cation binding site of BPAO as the most significant structural features controlling binding affinity. Structure-based design further ensured a high level of selectivity: ANETA is a good substrate of BPAO, but is not a substrate of either porcine kidney diamine oxidase (pkDAO) or rat liver monoamine oxidase (MAO-B). ANETA represents the first highly sensitive, selective, and tight binding fluorogenic substrate of a copper amine oxidase that is able to respond *directly* to the enzyme activity *in real time*.

Introduction

Copper amine oxidases (CAOs, EC 1.4.3.6) are a large family of copper-containing quinone-dependent amine oxidases which can be found in all living organisms including bacteria, yeast, plant and mammals.[1] The human versions of CAOs include semicarbazide sensitive amine oxidase (SSAO), diamine oxidase (DAO), and lysyl oxidase (LO).[2] Most CAOs use an active-site tyrosine-derived 2,4,5-trihydroxyphenylalanine quinone (TPQ) cofactor to catalyze oxidative deamination of unbranched primary amines to aldehydes and ammonia at the expense of reducing O_2 to H_2O_2.[1,3] Substrate turnover by CAOs follows a typical redox ping-pong mechanism (Scheme 1).[5] In the reductive half reaction, the TPQ cofactor is reduced to an aminoresorcinol concomitant with oxidative deamination of amine to aldehyde, the key step being conversion of substrate Schiff base (SSB) to product Schiff base (PSB) promoted by a highly conserved active site Asp residue. In the oxidative half reaction, the reduced aminoresorcinol cofactor is oxidized to an iminoquinone at the expense of reduction of O_2 to H_2O_2, with the iminoquinone subsequently undergoing hydrolysis to regenerate the resting TPQ with release of ammonia.[5]

The physiological importance of CAOs is still being defined. Human CAOs have been implicated in a number of diseases, including atherosclerosis, cardiovascular diseases, diabetes, Alzheimer's disease and cancer.[2] Recently, the human vascular endothelial SSAO/

Dr. Ke-Qing Ling, Current address: Department of Medicinal Chemistry, Ricerca Biosciences, LLC, Concord, OH 44077, e-mail: kqling@hotmail.com
Dr. Lawrence M. Sayre, Department of Chemistry, Case Western Reserve University, Cleveland, OH 44106, (216) 368-3704, (216) 368-3006 (FAX), e-mail: lms3@case.edu

vascular adhesion protein-1 (VAP-1) was identified as a novel target for developing drugs that may intervene in diabetes[6] and inflammatory diseases.[7] We have been interested in developing suicide inhibitors of CAOs as probes of mechanism and as potential lead compounds for pharmaceutical applications.[8] To study the kinetic behavior of highly potent inhibitors of the CAO bovine plasma amine oxidase (BPAO), we sought a sensitive and real time assay to monitor low levels of enzyme activity. The most sensitive assay for CAOs is the fluorometric coupled assay which monitors generation of H_2O_2during substrate turnover using horseradish peroxidase (HRP) as a secondary detecting enzyme.[9] However, HRP coupled assays may suffer from interferences arising from ancillary peroxide-forming reactions and possible direct interactions of the test inhibitor with HRP.[9,10] Moreover, the organic substrate for the HRP-H_2O_2 reaction may interact with CAOs and cause artifacts.[9,10]

In contrast to coupled assays, enzyme assays based on chromogenic and fluorogenic substrates provide a more direct connection between the enzyme activity and the optical signal, and are more resistant to artifacts.[11] The most widely used assay for CAOs such as BPAO utilizes benzylamine (BA) as a chromogenic substrate, which reports enzyme activity through the generation of benzaldehyde.[8,12] However, the spectrophotometric BA assay is insufficiently sensitive to allow for kinetic studies of highly potent BPAO inhibitors using low enzyme concentrations. Moreover, since the BA assay operates at short wavelength (250 nm), it can suffer from interferences of UV-active inhibitors or turnover products derived therefrom. Also, because of the large K_m of BA with BPAO, the required use of high BA concentrations to achieve saturation results in a rather high substrate background at 250 nm.[12]

Reported herein is our effort to develop a sensitive, selective, and tight-binding fluorogenic substrate of BPAO. A lead compound with suitable molecular geometry and optical properties was first identified. Further development was directed at building in structural features that conferred high binding affinity as determined by computer-aided analysis of substrate docking into the known BPAO crystal structure. A series of extremely tight binding substrates of BPAO was discovered, among which a novel substrate with a nanomolar K_m and a sufficiently high k_{cat} was identified. This substrate is by far the most sensitive and tight-binding fluorogenic substrate of BPAO that responds *directly* to the enzyme activity *in real time*. Moreover, since this compound was tailored specifically for BPAO, impressive selectivity among different amine oxidases was observed. The high sensitivity of the new substrate with BPAO permitted development of a fluorometric non-coupled assay for evaluating BPAO activity at nanomolar concentrations, thereby permitting evaluation of IC_{50} values in the nanomolar range for highly potent inhibitors.

Results and discussion

Identification of lead compound

An ideal fluorophore for a fluorogenic substrate should absorb/emit at wavelengths long enough to avoid interference from protein background at 220 and 280 nm, but at the same time not be too bulky for the enzyme to accommodate. We chose the medium-sized and linearly shaped naphthalenemethaneamines **1** and **2** as the first generation fluorogenic substrates of BPAO, which are expected to respond directly to the enzyme activity in real time by generation of aldehyde turnover products **3** and **4**,[13] whose $\lambda_{max}/\lambda_{em}$ characteristics are 313/460 and 377/530 nm, respectively. These fluorophores have been employed previously in developing fluorescence sensors of aldolase antibodies.[14a] The O and N substituents confer a “push-pull” electronic effect in the product aldehydes, giving rise to large Stokes’ shifts and significantly increased fluorescence intensities compared to 2-naphthaldehyde.[15]

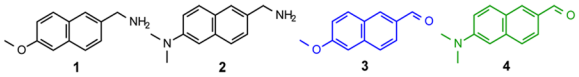

Metabolism of compounds **1** and **2** by BPAO was followed by UV-vis and fluorescence spectrophotometry (Figure 1 and Figure 2). The excitation wavelengths for fluorescence measurements were chosen on the basis of optimizing the absorbance of product aldehydes relative to absorbance of starting amines. Both compounds were well-behaved substrates as indicated by the linear time dependence of Δ*A*. However, despite comparable absorbance signals for **1** and **2**, the finding that the fluorescence signal generated from metabolism of **2** was significantly weaker than that from metabolism of **1**, led us to exclude **2** and focus on **1** as the lead fluorogenic substrate for further development.

Structure-based design

Although **1** was a fairly good substrate of BPAO, its application was limited due to low binding affinity and poor solubility. To develop improved fluorogenic substrates, we pursued a structure-based design with **1** as scaffold. Native BPAO has a funnel-shaped active site (Figure 3).[16] Three carboxylic residues, Asp179, Asp445 and Glu417, are located around the active site mouth opening. Inside the active site, there is a hydrophobic pocket defined by Tyr175, Tyr383, Phe388, Phe393, Met467, and Leu468, while further inside are located the TPQ cofactor (TPQ470), the catalytic general base Asp385, and the copper(II) coordinated to His519, His521 and His683 (Figure 3). In the best scored productive docking mode of **1** with BPAO, the substrate amino group is interacting with Asp385 by hydrogen bonding, while the naphthalene ring and the methyl group of **1** are interacting with the hydrophobic pocket (Figure 3). On the basis of this binding model, it is obvious that branching on the naphthalene ring of **1** would cause steric problems. However, since the MeO group of **1** is pointing towards the active site mouth opening where no critical steric constraints exist (Figure 3), we felt comfortable making structural modifications at this position. Compounds *5 – 7* were thus designed as second-generation substrates.[17] Both **5** and **7** showed much improved solubility compared to **1**.

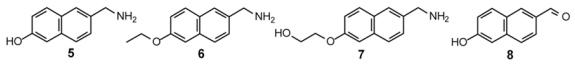

Screening of compounds **5 – 7** revealed that compound **7** was an exceptionally tight binding substrate of BPAO, but its k_{cat} was small (Table 1). Thus, further development was conducted based on**7**. Docking simulation showed that, while the naphthalenemethaneamine portion of **7** is interacting with Asp385 and the hydrophobic pocket in a similar manner as seen in **1**, the OH of **7** is interacting with Asp445 at the active site mouth rim, which might contribute to the low K_m of **7** (Figure 4). This is particularly interesting because Asp445 has been previously proposed as a secondary cation binding site to account for the low K_m of polyamine substrates such as spermine and spermidine with BPAO.[16,18] Recent studies in our lab revealed that two other residues (Asp179 and Glu 417) at the active site mouth rim of BPAO, may also constitute ancillary cation binding sites.[19] It then seemed obvious to replace the OH group of **7** with an amino group, which in protonated form could interact strongly with Asp445. Substrate optimization was approached by fine-tuning the tether length between the amino group and aryl ether oxygen, as well as methylating the amino group to generate secondary, tertiary, or quaternary derivatives. Thus, compounds **9–16** were designed as the third generation substrates. We chose to study only the tertiary and quaternary amine versions of C_3 and C_4 tether diamine substrates because **9** and **10** turned out to be inferior substrates of BPAO (Table 1). All these diamine substrates are highly soluble under physiological conditions.

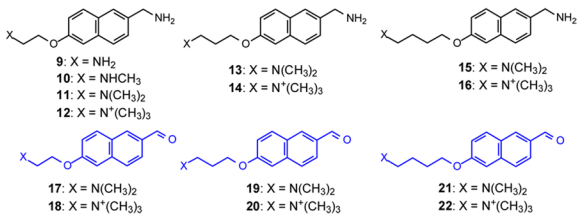

Synthesis

Syntheses of compounds **1**, **2** and **4–8** are described in Experimental Section and Supporting Information. Syntheses of the C_2 tether diamine substrate series **9–12**, along with two aldehydes **17** and **18**, were achieved by a highly convergent synthetic strategy (Scheme 2). Thus, coupling **23** with Boc protected 2-aminoethyl bromide, followed by deprotection of the coupling product **24**, yielded the key intermediate **25**. $LiAlH_4$ (LAH) reduction of **25** gave **9**. Formylation of **25**, followed by LAH reduction of the amide **26**, afforded **10**. Reductive methylation of **25** with CH_2O led to the tertiary amine **27**, which was reduced with LAH to give **11**. Boc protection of **11**, followed by quaternization of **28** with MeI, anion exchange with Ag_2CO_3, and deprotection with aqueous HCl, gave $_{12}$. On the other hand, reduction of **27** with DIBAL-H afforded aldehyde **17**. The latter was quaternized with MeI to give aldehyde **18**. Following the same strategy, the C_3 tether diamine substrates **13** and **14**, and the corresponding aldehydes **19** and **20** were also synthesized (Supporting Information). However, application of the same strategy to the syntheses of the C_4 tether diamine substrates **15** and **16** resulted in a poor yield. While this reaction was still employed to prepare small amounts of the authentic aldehydes **21** and **22**, **15** and **16** were obtained through a different synthetic route (Supporting Information).

Metabolism

Metabolism of the new substrates by BPAO all resulted in spontaneous UV-vis and/or fluorescence signal changes (see Figure 5 for an example). The spectral changes matched those of authentic samples of the expected turnover products, in cases where these were available synthetically (Figure 1, Figure 2 and Figure 5). In selected cases, we also established precursor-product relationships through HPLC analysis. For example, metabolism of substrate **12** by BPAO resulted in time-dependent formation of a single species, which was identical with authentic aldehyde **18** in both HPLC retention time and diode array difference (DAD) spectral properties (Figure 6). Similar results were also observed in HPLC analysis of the metabolism of **1** (Figure S11). It seems reasonable to conclude that the observed optical changes during metabolism of all the substrate analogs are due to clean conversion to the corresponding aldehydes.

Optical properties of turnover products

To determine the kinetics of substrate probe turnover using fluorescence spectrometry, the concentration of turnover products must be determined based on the relative fluorescence intensities. These data and the measured excitation and emission wavelengths for the commercially available turnover aldehyde **3** of lead compound **1** and for eight other aldehydes synthesized independently, are listed in Table S1. For the 6-oxy-substituted-2-naphthaldehydes, the ratios of relative fluorescence intensity with respect to that of **3** ranged from 0.87 to 1.08, suggesting only modest effects of distal substitutions on the electronic property of the core fluorophore. In the four other cases, the relative fluorescence intensity was estimated (see Supporting Information) according to the trends observed for the synthetic compounds in hand.

Possible quenching of selected aldehydes by several relevant species was also examined. No detectable quenching was observed when aldehydes **17** or **18** were mixed with up to 10 nM of BPAO or with 10 μM of the corresponding substrates **11** or **12**, viz. despite changes in the emission backgrounds, the slopes of the calibration curves (AU/nM) of the aldehydes in the absence and presence of enzyme or corresponding substrate were identical within experimental error (Figure S13 and Figure S14).

Evaluation of substrate activity

Substrate activities of all the new synthetic primary amines for BPAO were evaluated relative to BA. By monitoring turnover products with UV-vis or fluorescence spectrophotometry, the initial oxidation velocity (V_0) was measured as a function of substrate concentration (Figure 7 and Figure S15). Non-linear least squares fits of the V_0-[S] plots to the Michaelis-Menten equation $V_0 = k_{cat}$ [E]/(1+K_m/[S]) afforded the K_m and k_{cat} values listed in Table 1. To assess the reliability of the fluorometric method, which is known to be susceptible to interferences from various factors, the substrate parameters of **1** were determined by both UV-vis and fluorescence spectrophotometry using quite difference enzyme concentrations. The results agreed well with each other (Table 1). For substrate **9**, despite the fact that both amine termini could potentially be metabolized by BPAO, the measured parameters only reflect metabolism at the chromogenic benzylic amine position.

Structure-activity relationship (SAR)

Data in Table 1 reveal several interesting SAR aspects. The fact that compounds **1**, **2** and **6** all possess smaller K_m values than that of BA suggests that there is no steric problem for the enzyme to accommodate a naphthalene ring, and that increasing substrate hydrophobicity appears to favor binding. This is consistent with docking studies suggesting that all our substrates bind to BPAO in a way where the naphthalene ring is being held within the active site hydrophobic pocket (Figure 3, Figure 4, Figure 8 and Figure S1–S10). The most compelling finding by far was that the third generation diamine substrates **9–16** all have K_m values 3–4 orders of magnitude smaller than those of monoamine substrates (Table 1). Consistently, the best-scored productive docking modes for these diamine substrates all involve an additional interaction (hydrogen bonding and electrostatic attraction) between the ancillary amino group and Asp445 or Asp179 at the mouth opening of the active site (Figure 8 and Figure S4–S10).[20] The strength of this additional interaction is indicated by the significantly higher docking scores (1.63–3.42) seen for the diamines than for the monoamines (0.04–0.65) (Table 1). Also, there is an apparent decrease in K_m going from the C_2 tether to the C_4 tether, suggesting that longer tether diamines can better achieve favorable interactions in the enzyme active site fit. The fact that all the quaternary ammonium substrates have smaller K_m values than the corresponding tertiary amine substrates suggests that a permanent charge on the second amino group is more favorable for binding than a dissociable ammonium group. However, the differences are not large, and it should be noted in the C_2 series that there is significant variation in K_m among the 1°,2° and 3° amino substrates.

As far as k_{cat} is concerned, the variation observed is much less than for K_m. BA and **5**, the two substrates with the highest K_m values, have the highest k_{cat} values, 50–75-fold higher than the slowest substrates **9** and **16** (Table 1). It is well known that there are often compensatory changes in K_m and k_{cat}. In our case, small k_{cat} values for tight-binding substrates with extended structures may reflect in part a decreased maneuverability, and that aldehyde turnover products may also bind tightly and escape only slowly from the active site.[21] The fact that **7** and all the diamine substrates have smaller k_{cat} values than does **1** further supports this notion, because binding of the OH or the second amino group at the ancillary cation binding sites would decrease the maneuverability of substrate and turnover product. As for the dependence of k_{cat} on the tether length of the diamine substrates, there is a moderate decrease in k_{cat} from

C_2 to C_3, and a nearly 10-fold decrease in k_{cat} from C_3 to C_4 (Table 1). This is also consistent with a role of increasing bulk and decreasing maneuverability of substrates and turnover products in governing k_{cat}.

Substrate "goodness" is assessed in terms of k_{cat}/K_m (Table 1). Thus, except for **5**, all other compounds are better substrates of BPAO than BA, with the k_{cat}/K_m of **10–14** being more than three orders of magnitude larger than that of BA. However, in choosing a suitable fluorogenic substrate of BPAO, both K_m and k_{cat} must be taken into account. The best compromise would bea substrate with a K_m low enough to allow achieving saturation at as low a concentration as possible, and a k_{cat} large enough to ensure sensitivity. Thus, (2-(6-(aminomethyl)naphthalen-2-yloxy)ethyl)trimethylammonium (**12**, ANETA) was selected as the optimal fluorogenic substratefor BPAO among those compounds evaluated here.

Selectivity of the new fluorogenic substrate

Because **12** was developed through structural design specifically for BPAO, it should be a selective substrate for BPAO relative to other amine oxidases. The initial oxidation velocities of **12** at 20 μM (100-fold the K_m for BPAO) for five amine oxidases, namely BPAO, porcine kidney diamine oxidase (pkDAO), *Arthrobacter globiformis* amine oxidase (AGAO), *Pichia pastoris* lysyl oxidase (PPLO), and rat liver monoamine oxidase (MAO-B), were measured by monitoring the formation of **18** at 250 nm. The enzyme concentrations were adjusted to achieve comparable specific activities against their normal substrates, *p*-xylylenediamine (PXDA) for pkDAO,[22] and BA for all other enzymes (Table 2).[8d,12] While **12** was metabolized quickly by BPAO, no significant substrate activity was observed with pkDAO, AGAO and MAO-B (Table 2). The only other enzyme that could metabolize **12** at a comparable rate was PPLO, a yeast CAO whose active site bears the closest topological and electrostatic resemblance to that of BPAO.[16] The high apparent selectivity of **12** for BPAO over MAO-B is particularly important because the latter is the major enzyme in mammalian tissues that interferes with studies of CAO activities using BA.

Application in BPAO inhibitor evaluation

An estimation of the potency of enzyme inhibitors in terms of IC_{50} values depends, as its lower limit, on the concentration of enzyme used in the analysis (e.g., even for "stoichiometric" inhibitors, one cannot measure an IC_{50} value that is less than half the enzyme concentration). The development of a tight-binding, sensitive substrate thus permits assay of very low enzyme concentrations, thus enabling estimation of truer IC_{50} values for very potent inhibitors. In this regard, we developed an optimized fluorometric assay protocol involving incubation of **12** (10 μM, 50-fold the K_m) with BPAO in 0.1 M of pH 7.2 phosphate buffer at 30 °C, and monitoring the fluorescence signal at 453 nm for 30 s (λ_{ex} 350 nm). Under such conditions, an excellent linear relationship was observed between initial oxidation velocity (V_0) and the concentration of BPAO in the range of 0–10 nM (Figure 9). At 5 nM BPAO (Figure S16), the slope of fluorescence growth at 453 nm (6.33 AU/s) is more than three orders of magnitude higher than the background slope (0.0061±0.010 AU/s), thereby providing an optical signal that is strong enough for conduct of kinetic studies of potent BPAO inhibitors. The detection limit (blank mean+3SD) of the new fluorometric assay is 0.03 nM, two orders of magnitude lower than for the BA assay (3 nM). Moreover, the excitation and emission wavelengths (350 and 453 nm) used by the new assay are in the near UV and visible region, respectively, thereby avoiding interferences often met when using BA assay.

1-Amino-2,3-butadiene (**29**) is one of the most potent mechanism-based inhibitors of BPAO reported to date, and we resorted to low temperature to define the kinetics of inactivation (with standard enzyme concentrations used in the BA spectrophotometric assay), without having to utilize stopped-flow techniques.[8d] Using our new fluorometric assay (**12** as substrate), we first

were able to reproduce the kinetics of inactivation of BPAO by **29** at 2 °C (Figure 10). The calculated slope of the Kitz and Wilson plot (10.8) matches that obtained using the BA assay (10.2) (Figure 10).[8d] This helps to validate **12** as a reliable substrate to evaluate inhibitors of BPAO. Moreover, since enzyme concentration is reduced in the new assay to nanomolar levels, the concentration of inhibitors can also be reduced to this level in an effort to get a better sense of their potency. With the new assay, the kinetic behavior of **29** with BPAO could be easily studied at 30 °C (Figure S18), and a k_{inact}/K_i of 553±7 mM^{-1} min^{-1} at 30 °C was obtained from the Kitz and Wilson plot. Furthermore, the 5 and 10 min IC_{50} values at 30 °C could be determined as 250 nM and 125 nM, respectively. Our previous estimation of the 5 min IC_{50} of **29** using the BA assay with 1 μM BPAO was 1.25 μM.[8d]

Conclusion

We have developed a novel fluorogenic substrate of BPAO by structure-based design. Computer-aided docking simulations permitted us to recognize the ancillary cation binding domain as the most useful structural feature of BPAO that controls binding affinity. This led to the discovery of a series of extremely tight binding substrates, among which **12** was identified as an optimal fluorogenic substrate of BPAO. The use of structure-based rational design helped to ensure that **12** would exhibit impressive selectivity for BPAO over two other mammalian amine oxidases tested. Moreover, the observed SAR in our synthetic substrate library also provides important information about substrate specificity of BPAO. All the information generated in this study should be useful in future substrate/inhibitor design. To our knowledge, compound **12** is the first highly sensitive, tight binding, and selective fluorogenic substrate of a CAO that can respond directly to the enzyme activity in real time. The high affinity of **12** allowed us to develop a fluorometric non-coupled assay that can be used to evaluate BPAO inhibitors at nanomolar levels. Compounds of this type could serve as sensors of copper amine oxidase activities in biological tissues.

Experimental

6-Methoxy-2-naphthalenemethaneamine hydrochloride (1·HCl)

To a suspension of 1.9 g (50 mmol) of LAH in 200 mL of Et_2O was slowly added with vigorous stirring at 0 °C a solution of 6-methoxy-2-naphthonitrile (3.66 g, 20 mmol) in 100 mL of Et_2O. The mixture was stirred at room temperature for 4 h, at which point 10 mL of EtOAc was added dropwise with cooling at −78 °C to decompose excess LAH. The final mixture was slowly added to a mixture of ice (500 g) and sodium tartrate (10 g) under stirring. The organic layer was separated, and the aqueous layer was saturated with solid NaCl and extracted with Et_2O (3×100 mL). The combined organic layers were dried (Na_2SO_4), the solvent was evaporated, and the residue was dissolved in 20 mL of 12 *N* aqueous HCl. Evaporation of solvent and crystallization of the residue from EtOH-*i*PrOH afforded pure **1** HCl (3.89 g, 17 mmol, 85%): white plates, mp 279–280 °C (decomp); ^{1}H NMR (CD_3OD) δ 3.86 (s, 3H), 4.25 (s, 2H), 7.14 (dd, 1H, *J* = 2.4, 8.8 Hz), 7.22 (d, 1H, *J* = 2.0 Hz), 7.52 (dd, 1H, *J* = 1.6, 8.8 Hz), 7.79 (d, 1H, *J* = 9.2 Hz), 7.82 (d, 1H, *J* = 8.4 Hz), 18 7.87 (s, 1H); ^{13}C NMR (CD_3OD) δ 44.4, 56.0, 106.8, 120.2, 127.6, 129.0, 129.2, 129.3, 129.9, 130.6, 135.9, 159.4; HRMS (FAB) *m/z* calcd for $C_{12}H_{14}NO$ (MH^+) 188.1075, found 188.1077.

2-(6-(Aminomethyl)naphthalen-2-yloxy)ethylamine dihydrochloride (9·2HCl)

A mixture of 2-bromoethylamine HBr (8.20 g, 40 mmol), di-*tert*-butyl dicarbonate (8.72 g, 40 mmol), and diiospropylethylamine (DIEA, 20 mL) in 200 mL of CH_2Cl_2 was stirred at room temperature overnight. The solvent was evaporated at room temperature and the residue was extracted with 200 mL of Et_2O. The solid material was filtered off and washed with Et_2O. The

combined filtrates were evaporated to dryness to afford crude (2-bromoethyl)carbamic acid *tert*-butyl ester as a light brown oil, which solidified over time (7.6 g, 34 mmol, 85%).

A mixture of 6-cyano-2-naphthol (5.07 g, 30 mmol), (2-bromoethyl)carbamic acid *tert*-butyl ester (6.72 g, 30 mmol), anhydrous K_2CO_3 (4.14 g, 30 mmol), and KI (4.98 g, 30 mmol) in 100 mL of dry DMF was stirred under argon at 50 °C for 24 h. The mixture was partitioned between 1 L of CH_2Cl_2 and 1 L of 5% aqueous K_2CO_3. The organic layer was separated, washed with 5% aqueous K_2CO_3 (3×100 mL), dried (Na_2SO_4), and evaporated to dryness to give crude [2-(6-cyanonaphthalen-2-yloxy)ethyl]carbamic acid *tert*-butyl ester (**24**) as a light brown oil which solidified on standing.

The latter was dissolved into 50 mL of dry trifluoroacetic acid (TFA) with cooling at 0 °C. The solution was stirred at room temperature for 20 min and then evaporated to dryness to give crude 6-(2-aminoethoxy)naphthalene-2-carbonitrile **25** CF_3CO_2H as a brown oil (9.6 g, 29.4 mmol, 98%).

A suspension of **25** CF_3CO_2H (1.63 g, 5 mmol) in 100 mL of absolute Et_2O was treated with LAH (1.9 g, 50 mmol) as above. The excess LAH was decomposed with EtOAc and the resulting mixture was further treated with ice and sodium tartrate. The organic layer was separated. The aqueous layer was saturated with solid NaCl, and extracted with Et_2O (3×50 mL). The combined organic layers were extracted with 100 mL of 0.5 *N* aqueous HCl. The aqueous layer was separated, washed with Et_2O (2×50 mL), brought to pH 11 with NaOH, saturated with solid NaCl, and extracted with Et_2O (3×100 mL). The latter organic layers were collected, dried (Na_2SO_4), and evaporated to dryness. The residue was dissolved in 10 mL of 12 *N* aqueous HCl, and then evaporated to dryness. The final residue was crystallized from EtOH-MeOH to afford pure **9** 2HCl as a white powder (0.67 g, 2.3 mmol, 46%): mp >360 °C (decomp); ^{1}H NMR (CD_3OD) δ 3.45 (t, 2H, *J* = 5.0 Hz), 4.26 (s, 2H), 4.39 (t, 2H, *J* = 5.0 Hz), 7.23 (dd, 1H, *J* = 2.4, 8.8 Hz), 7.28 (d, 1H, *J* = 2.4 Hz), 7.51 (dd, 1H, *J* = 1.6, 8.4 Hz), 7.81 (d, 1H, *J* = 8.8 Hz), 7.84 (d, 1H, *J* = 8.8 Hz), 7.88 (s, 1H); ^{13}C NMR (CD_3OD) δ 40.3, 44.5, 65.4, 108.0, 120.5, 127.8, 129.2, 129.4, 130.0, 130.6, 130.9, 136.1, 158.2; HRMS (FAB) *m/z* calcd $C_{13}H_{17}N_2O$ (MH^+) 217.1341, found 217.1342.

(2-(6-(Aminomethyl)naphthalen-2-yloxy)ethyl)methylamine dihydrochloride (10·2HCl)

The mixed anhydride of formic and acetic acids was first prepared by stirring a mixture of acetic anhydride (0.561 g, 5.5 mmol), formic acid (0.253 g, 5.5 mmol), and pyridine (0.435 g, 5.5 mmol) in 10 mL of dry CH_2Cl_2 at room temperature for 1 h. To the resulting mixture was added a solution of the above crude **25** CF_3CO_2H (1.63 g, 5 mmol) and Et_3N (2.02 g, 20 mmol) in CH_2Cl_2 (10 mL). The mixture was stirred at room temperature for 1 h, diluted with Et_2O to 200 mL, and then washed with brine (3×50 mL). The organic layer was separated, dried (Na_2SO_4), and evaporated to dryness to give crude 6-(2-formamidoethoxy)naphthalene-2-carbonitrile (**26**) as a brown oil.

The above crude **26** was reduced with LAH in Et_2O and worked up exactly as for **25** above, including purification of the final HCl salt, affording pure **10** 2HCl as a white powder (0.62 g, 2.04 mmol, an overall yield of 41%): mp 304–306 °C (decomp); ^{1}H NMR (D_2O/CD_3OD) δ 2.84 (s, 3H), 3.54 (t, 2H, *J* = 4.8 Hz), 4.29 (s, 2H), 4.41 (t, 2H, *J* = 4.8 Hz), 7.30 (dd, 1H, *J* = 2.4, 9.2 Hz), 7.36 (d, 1H, *J* = 2.4 Hz), 7.52 (d, 1H, *J* = 8.8 Hz), 7.86–7.92 (3H); ^{13}C NMR (D_2O/CD_3OD) δ 33.8, 44.2, 49.0, 63.9, 107.9, 120.1, 127.7, 129.0, 129.2, 129.3, 129.9, 130.9, 135.3, 157.3; HRMS (FAB) *m/z* calcd $C_{14}H_{19}N_2O$ (MH^+) 231.1497, found 231.1492.

6-(2-(Dimethylamino)ethoxy)naphthalene-2-carbonitrile (27)

To a solution of **25** CF_3CO_2H (5.87 g, 18 mmol), glacial HOAc (10 mL), and 37% aqueous CH_2O (3 mL, 40 mmol) in 100 mL of MeOH was added in small portions solid $NaCNBH_3$ (3.15 g, 50 mmol) with vigorous stirring and cooling to 0 °C. The mixture was then stirred at room temperature for 2 h and MeOH was evaporated. The residual solution was diluted with 200 mL of brine, neutralized with solid $NaHCO_3$ to pH 7, basified with NaOH to pH 11, and extracted with EtOAc (3×200 mL). The combined organic layers were extracted with 200 mL of 0.5 *N* aqueous HCl. The aqueous layer was separated, washed with Et_2O (2×50 mL), neutralized with solid $NaHCO_3$ to pH 7, brought to pH 11 with NaOH, saturated with solid NaCl, and extracted with EtOAc (3×100 20 mL). The latter organic layers were collected, dried (Na_2SO_4), and evaporated to dryness to give **27** as a brown viscous oil (2.64 g, 11.0 mmol, 61%): ^{1}H NMR ($CDCl_3$) δ 2.36 (s, 6H), 2.80 (t, 2H, *J* = 5.6 Hz), 4.19 (t, 2H, *J* = 5.6 Hz), 7.14 (d, 1H, *J* = 2.0 Hz), 7.27 (dd, 1H, *J* = 2.0, 9.2 Hz), 7.53 (dd, 1H, *J* = 1.2, 8.4 Hz), 7.74 (s, 1H), 7.75 (d, 1H, *J* = 9.2 Hz), 8.10 (s, 1H); ^{13}C NMR ($CDCl_3$) δ 46.1, 58.3, 66.3, 106.7, 106.8, 119.8, 121.2, 127.2, 127.86, 127.94, 130.1, 133.9, 136.5, 159.4.

(2-(6-(Aminomethyl)naphthalen-2-yloxy)ethyl)dimethylamine dihydrochloride (11·2HCl)

A solution of **27** (2.00 g, 8.3 mmol) was reduced with LAH (1.14 g, 30 mmol) in Et_2O and worked up exactly as for **25** above, including purification of the final HCl salt, affording pure **11** 2HCl as a white solid (2.02 g, 6.4 mmol, 77%): mp 274–276 °C (decomp); ^{1}H NMR (CD_3OD) δ 3.03 (s, 6H), 3.70 (t, 2H, *J* = 4.8 Hz), 4.27 (s, 2H), 4.52 (t, 2H, *J* = 4.8 Hz), 7.33 (dd, 1H, *J* = 2.8, 9.2 Hz), 7.43 (d, 1H, *J* = 2.8 Hz), 7.56 (dd, 1H, *J* = 2.0, 8.4 Hz), 7.88 (d, 1H, *J* = 8.8 Hz), 7.91 (d, 1H, *J* = 8.8 Hz), 7.93 (s, 1H); ^{13}C NMR (CD_3OD) δ 44.0, 44.5, 58.0, 63.3, 108.3, 120.5, 127.9, 129.2, 129.5, 130.1, 130.7, 131.0, 136.0, 157.8; HRMS (FAB) *m/z* calcd $C_{15}H_{21}N_2O$ (MH^+) 245.1654, found 245.1642.

(2-(6-(Aminomethyl)naphthalen-2-yloxy)ethyl)trimethylammonium chloride hydrochloride (12Cl$^-$·HCl)

A mixture of **11** 2HCl (1.00 g, 3.15 mmol), Et_3N (5 mL), and di-*tert*-butyl dicarbonate (0.70 g, 3.21 mmol) in 50 mL dry CH_2Cl_2 was stirred at room temperature overnight. The solvent was evaporated at room temperature, and the residue was partitioned between 100 mL of Et_2O and 100 mL of alkaline brine (pH 11). The organic layer was separated, washed with alkaline brine (3×50 mL), dried (Na_2SO_4), and evaporated to dryness to give (6-(2-dimethylaminoethoxy)naphthalen-2-ylmethyl)carbamic acid *tert*-butyl ester (**28**) as a colorless oil.

The latter oil was dissolved in 10 mL of absolute Et_2O and the solution was filtered. To the clear filtrate was added iodomethane (0.71 g, 5 mmol). After mixing thoroughly, the solution was sealed and was allowed to stand at room temperature overnight. The precipitates were collected, washed with Et_2O and dried to give (2-(6-(*tert*-butoxycarbonylaminomethyl) naphthalen-2-yloxy)ethyl)trimethylammonium iodide as a light yellow solid.

The latter solid was dissolved in MeOH (20 mL), followed by addition of finely ground solid Ag_2CO_3 (1.4 g, 5.1 mmol). The mixture was stirred at room temperature for 1 h, at which point, the $AgNO_3$ test showed the absence of iodide in the solution. The solid material was filtered off and washed with MeOH. To the combined filtrates was added 50 mL of 12 *N* aqueous HCl. The mixture was heated at 60 °C for 30 min and then evaporated to dryness to afford pure **12Cl**$^-$ HCl as a light yellow solid (881 mg, 2.99 mmol, 95%): mp 261–263 °C (decomp); ^{1}H NMR (CD_3OD) δ 3.33 (s, 9H), 3.96 (br, 2H), 4.27 (s, 2H), 4.65 (br, 2H), 7.28 (dd, 1H, *J* = 2.4, 8.8 Hz), 7.45 (d, 1H, *J* = 2.0 Hz), 7.56 (dd, 1H, *J* = 1.6, 8.8 Hz), 7.88 (d, 1H, *J* = 8.8 Hz), 7.92 (d, 1H, *J* = 8.8 Hz), 7.93 (s, 1H); ^{13}C NMR (CD_3OD) δ 44.5, 54.9, 63.3, 66.5, 108.4, 120.4,

127.9, 129.2, 129.5, 130.1, 130.8, 131.0, 136.0, 157.6; HRMS (FAB) *m/z* calcd $C_{16}H_{23}N_2O$ (M^+) 259.1810, found 259.1814.

6-(2-(Dimethylamino)ethoxy)naphthalene-2-carboxaldehyde (17)

To a solution of **27** (500 mg, 2.08 mmol) in 20 mL of dry CH_2Cl_2 was added under argon and electromagnetic stirring 1.4 mL (2.1 mmol) of 1.5 M DIBAL-H in toluene at room temperature. The mixture was stirred for 1 h, and then checked by TLC. Since the nitrile and aldehyde coelute on a silica gel column, it was necessary to achieve complete reduction of the former by titration with additional DIBAL-H. To the final reaction mixture was added 50 mL of 0.5 N aqueous HCl. The mixture was stirred at room temperature for 30 min and then neutralized with solid $NaHCO_3$ to pH 7. To this was added 1 g of sodium tartrate under stirring, and the resulting mixture was brought to pH 11 with NaOH, and then saturated with solid NaCl. The organic layer was separated, and the aqueous layer was extracted with CH_2Cl_2 (2×50 mL). The combined organic layers were dried (Na_2SO_4) and evaporated to dryness to leave a residue that was purified by silica gel column chromatography, eluting with EtOAc-hexanes containing 5% methanolic ammonia, to afford pure **17** as a light brown viscous oil which solidified on standing (397 mg, 1.63 mmol, 78%): mp 50–52 °C; ^{1}H NMR ($CDCl_3$) δ 2.33 (s, 6H), 2.77 (t, 2H, *J* = 5.6 Hz), 4.16 (t, 2H, *J* = 5.6 Hz), 7.13 (d, 1H, *J* = 2.0 Hz), 7.23 (dd, 1H, *J* = 2.6, 8.8 Hz), 7.73 (d, 1H, *J* = 8.4 Hz), 7.81 (d, 1H, *J* = 9.2 Hz), 7.85 (dd, 1H, *J* = 1.6, 8.4 Hz), 8.17 (s, 1H), 10.02 (s, 1H, CHO); ^{13}C NMR ($CDCl_3$) δ 45.9, 58.2, 66.2, 106.8, 120.3, 123.5, 127.8, 127.9, 131.1, 132.3, 134.3, 138.2, 159.5, 192.0; HRMS (FAB) *m/z* calcd $C_{15}H_{18}NO_2$ (MH^+) 244.1338, found 244.1338.

(2-(6-Formylnaphthalen-2-yloxy)ethyl)trimethylammonium iodide (18I$^-$)

A sample of the above **17** (200 mg, 0.82 mmol) was dissolved in 5 mL of absolute Et_2O. The solution was filtered. To the filtrate was added MeI (0.2 g, 1.4 mmol). After mixing thoroughly, the mixture was sealed and was allowed to stand at room temperature overnight. The precipitates were collected, washed with Et_2O and crystallized from MeOH to afford pure **18I**$^-$ (310 mg, 0.80 mmol, 98%): light yellow prisms, mp 193–195 °C; ^{1}H NMR (CD_3OD) δ 3.37 (s, 9H), 4.01 (m, 2H), 4.69 (m, 2H), 7.31 (dd, 1H, *J* = 2.4, 8.8 Hz), 7.47 (d, 1H, *J* = 2.4 Hz), 7.83 (dd, 1H, *J* = 1.6, 8.8 Hz), 7.88 (d, 1H, *J* = 8.4 Hz), 7.98 (d, 1H, *J* = 9.2 Hz), 8.32 (d, 1H, *J* = 0.8 Hz), 10.02 (d, 1H, *J* = 0.4 Hz, CHO); ^{13}C NMR (CD_3OD) δ 55.0, 63.5, 66.7, 108.9, 120.7, 124.2, 129.2, 129.9, 132.6, 134.2, 135.7, 139.5, 159.4, 194.0; HRMS (FAB) *m/z* calcd $C_{16}H_{20}NO_2$ (M^+) 258.1494, found 258.1489.

General procedures using amine oxidases

Purified samples of BPAO, AGAO, and PPLO were obtained as described in a previous study.[12] Porcine kidney diamine oxidase (pkDAO) was commercially available and had a specific activity of 0.08 unit/mg using putrescine as substrate. Rat liver mitochondria (MAO-B) were isolated and purified[23] as previously reported,[8d] and the protein concentration was determined by the biuret method with bovine serum albumin as standard.

The concentration of BPAO was determined from an estimate of the maximal units of activity in terms of active monomers,[24] which in our hands translates to the equation [BPAO] = slope × 86.2 ×dilution, where [BPAO] represents the concentration of the BPAO sample in μM; "slope" is defined as ΔA_{250} per second measured by UV spectrophotometry when an appropriate volume of enzyme sample was diluted into a 1 cm path-length cuvette containing 1 mL of 5 mM of BA and 50 mM of phosphate buffer (pH 7.2) at 30 °C. Concentrations measured this way are very close to those estimated by standard phenylhydrazine titration.[24] Purified BPAO samples were diluted to ca. 30 μM with 0.1 M pH 7.2 phosphate buffer as concentrated stock solutions, which can survive at least 10 freeze-thaw cycles without significant loss of activity. This stock was directly used in UV-vis measurements. For

fluorescence measurements, 1 μM stock solutions of BPAO, which lose significant activity at room temperature in 48 h, were made fresh everyday before use, and the 0.10 μM stock solution of BPAO was prepared immediately before use. Stock solutions of substrates and authentic turnover products (usually 25 or 50 mM) were prepared in water, or in dioxane if not water soluble. Dilute working solutions of suitable concentrations in water were made immediately before use. All the working solutions were filtered to remove any insoluble materials to ensure data quality.

Time dependent metabolism of substrates by BPAO followed by absorption spectroscopy

To a 1 mL/1 cm disposal cuvette were added 8 μL of a 2.5 mM stock solution of **12Cl**$^-$ HCl in water and 989 μL of 0.1 M of pH 7.2 phosphate buffer that had been maintained at 30 °C in a water bath. After addition of 3.1 μL of a 32.3 μM stock solution of BPAO, the solution was quickly mixed and subjected to UV-vis scanning every 30 s at 30 °C (Figure 5). Metabolism of compounds **1** and **2** by BPAO was monitored spectrophotometrically by the same procedure (Figure 1).

Time dependent metabolism of substrates by BPAO followed by fluorometry

To a 3 mL/1 cm quartz cuvette were added 12 μL of a 2.5 mM stock solution of **12Cl**$^-$ HCl in water and 2985 μL of 0.1 M of pH 7.2 phosphate buffer that had been maintained at 30 °C in a water bath. After addition of 3 μL of a 1.00 μM stock solution of BPAO, the solution was quickly mixed and subjected to fluorescence scanning every 1 min at 30 °C (Figure 5). The excitation wavelength was 350 nm. Metabolism of compounds **1** and **2** by BPAO was monitored fluorometrically by the same procedure (Figure 2).

HPLC characterization of substrate metabolism by BPAO

A mixture of 8 μL of a 25 mM stock solution of **12Cl**$^-$ HCl and 16 μL of a 12.5 mM stock solution of **18I**$^-$ was diluted to 1 mL with 0.1 M of pH 7.2 phosphate buffer, affording the authentic mixture solution. A 20 μL aliquot of this solution was subjected to HPLC analysis using a 4.6 × 250 mm Agilent SB C18, 5 μm column, a flow rate of 1 mL/min, and a gradient mobile phase composed of two HPLC-grade solvent mixtures: A [5% aqueous CH_3CN containing 0.02% (v/v) TFA] and B [95% aqueous CH_3CN containing 0.02% (v/v) TFA]. Using the solvent program 100%A 0–5 min, 100%A to 100%B 5–15 min, 100%B to 100% A 15–18 min, and 100% A 18–20 min, compounds **12** and **18** eluted with retention times of 3.4 and 12.3 min, respectively (Figure 6).

An 8 μL aliquot of a 25 mM stock solution of **12Cl**$^-$ HCl was diluted to 1 mL with 0.1 M of pH 7.2 phosphate buffer. After addition of 3.1 μL of a 32.3 μM stock solution of BPAO, the solution was mixed thoroughly at room temperature, and 20 μL aliquots were withdrawn periodically and analyzed by HPLC (Figure 6).

Experiments with **1** and **3** were conducted similarly except that the HPLC gradient mobile phase was programmed as follows: 100%A to 45%A (55%B) 0–10 min, 55%B to 100%B 10–20 min, 100%B to 100% A 20–22 min, and 100% A 22–24 min. Using this solvent program, compounds **1** and **3** had retention times of 9.4 and 15.0 min, respectively (Figure S11).

Evaluation of substrate activity

Reaction conditions for each of the substrates with BPAO were optimized (Table S2). In most cases the highly sensitive fluorometric method was used, to allow use of lower enzyme concentrations, thereby minimizing errors in rate measurements arising from a decrease in substrate concentration during the 30 s monitoring time period. The UV-vis method, which requires higher enzyme concentrations, was employed only in cases where metabolism-caused

decreases in substrate concentrations within 30 s were negligible. The excitation wavelengths for fluorescence measurements were optimized to ensure maximum emission intensities of turnover products and minimum substrate emission backgrounds. The monitoring wavelengths for UV-vis measurements were selected such that absorptions of substrates were negligible. Whereas 0.1 M pH 7.2 phosphate buffer was used in most cases, a reduced buffer concentration (33 mM) was chosen for poorly soluble substrates **1**, **2** and **6** to allow for collection of sufficient data. For each substrate, the order of magnitude of K_m was first estimated by measuring the turnover rates at a limited number of substrate concentrations, usually starting from 1 mM, and then reduced appropriately. On this basis, the operating substrate concentrations were decided.

A typical experiment using the UV-vis method proceeded as follows. To a 1 mL/1 cm disposal cuvette was added a prescribed volume of a stock solution of **2** HCl in water (5 or 50 mM). The cuvette was then filled to 994 μL with 33 mM pH 7.2 phosphate buffer that had been maintained at 30 °C in a water bath. After addition of 6.2 μL of a 32.3 μM stock solution of BPAO, the solution was quickly mixed and then subjected to UV-vis monitoring at 400 nm at 30 °C for 30 s. The time dependent ΔA_{400} traces were analyzed, and the slopes were converted to initial oxidation velocities (V_0) in terms of μM s^{-1} using the extinction coefficient of aldehyde **4** at 400 nm. The plot of V0 vs. [**2**] was constructed (Figure S15) and analyzed by non-linear least squares fit to the Michaelis-Menten equation to give K_m and k_{cat} values (Table 1).

A typical experiment using the fluorometric method proceeded as follows. To a 3 mL/1 cm quartz cuvette was added a prescribed volume of a stock solution of **12Cl**– HCl in water (0.025, 0.25, or 2.5 mM). The cuvette was then filled to 2994 μL with 0.1 M of pH 7.2 phosphate buffer that had been maintained at 30 °C in a water bath. After addition of 6.0 μL of a 1.00 μM stock solution of BPAO, the solution was quickly mixed and then subjected to fluorescence monitoring at 453 nm at 30 °C for 30 s with excitation at 350 nm. The time dependent ΔI_{453} traces were analyzed and the slopes were converted to the initial oxidation velocities (V_0) in terms of nM s^{-1} using the relative fluorescence intensity of aldehyde **18** at 453 nm. The K_M and k_{cat} data (Table 1) were obtained similarly from the plot of V_0vs. [**12**] (Figure 7).

Linearity between initial oxidation velocity and enzyme concentration

To a 3 mL/1 cm quartz cuvette containing 0.1 M pH 7.2 phosphate buffer at 30 °C were added 12 μL of a 2.5 mM stock solution of **12Cl**$^-$ HCl in water and an appropriate volume of 1.00 μM or 0.10 μM stock solution of BPAO. The final volume was 3000 μL. The final concentration of **12** was 10 μM, and the final concentration of enzyme was 0.10–10.0 nM. After quick mixing, the solution was subjected to fluorescence monitoring at 453 nm (λ_{ex} 350 nm) at 30 °C for 30 s. The collected slopes were converted to the initial oxidation velocities (V_0) in terms of nM s^{-1} as above, and then plotted against [BPAO] to give the calibration curves (Figure 9).

Selectivity of the new fluorogenic substrate

For BPAO, AGAO and PPLO, to a 1 mL/1 cm disposal cuvette was added 1000 μL of a stock solution of **12** (20 μM) in 0.1 M of pH 7.2 phosphate buffer, or 1000 μL of BA (5 mM) in 50 mM of pH 7.2 phosphate buffer at 30 °C. A minimum volume (5–10 μL) of an appropriate concentration of purified enzyme was diluted into the cuvette. After quick mixing, the solutions were subjected to UV monitoring at 250 nm at 30 °C for 30 s. The time dependent ΔA traces were analyzed and the slopes in terms of nM s^{-1} were calculated according to the extinction coefficients of **18** or PhCH=O at 250 nm (Table 2).

For pkDAO, to a 1 mL/1 cm disposal cuvette were added 250 μL of a stock solution of pkDAO (10 mg/mL) in 0.1 M of pH 7.2 phosphate buffer and 740 μL of 0.1 M of pH 7.2 phosphate

buffer. The solution was mixed and kept at 37 °C. A 10 μL aliquot of a stock solution of **12** (2.0 mM) or PXDA (0.15 M) in water was added. After quick mixing, the solutions were monitored at 250 nm at 37 °C for 30 s, and the slopes were calculated similarly as above, using a literature reported extinction coefficient for *p*-(aminomethyl)benzaldehyde[22] (Table 2).

For rat liver MAO-B,[8b] a 40 μL aliquot of a freshly thawed rat liver mitochondria suspension (66.6 mg/mL) in buffer (220 mM mannitol, 70 mM sucrose, 5 mM MOPS, pH 7.4) was diluted with 210 μL of 0.1 M of pH 7.2 phosphate buffer containing 0.25% of Triton X-100.The resulting homogenous solution was incubated at 30 °C. A 100 μL aliquot of this solution was diluted into 1000 μL of **12** (20 μM) in 0.1 M of pH 7.2 phosphate buffer, or 1000 μL of BA (5 mM) in 50 mM of pH 7.2 phosphate buffer at 30 °C. After quick mixing, the solutions were monitored at 250 nm at 30 °C for 30 s, and the slopes were calculated similarly (Table 2).

Optimized fluorometric assay protocol

To a 3 mL/1 cm quartz cuvette was added 2700 μL of a stock solution of **12** (11 μM) in 0.1 M pH 7.2 phosphate buffer that was stored in a 30 °C water bath. A 300 μL aliquot of a 50 nM stock solution of BPAO was diluted into the cuvette. After quick mixing, the solution was subjected to fluorescence monitoring at 453 nm (λ_{ex} 350 nm) at 30 °C for 30 s (Figure S16). The same experiment was repeated except that the 300 μL aliquot contained only buffer without BPAO. The time dependent ΔI_{453} traces were analyzed and the slopes were calculated.

Evaluation of inhibition of BPAO by 1-amino-2,3-butadiene (29) using the fluorometric assay

A solution of BPAO (50 nM) in 0.1 M of pH 7.2 phosphate buffer was incubated at 2 °C for 5 min. To it was added an appropriate volume of a prescribed concentration of **29** HCl in water (the final concentrations were 1–10 μM). The total volume of the incubation mixture was 3000 μL. Aliquots of the incubation mixture (300 μL) were withdrawn periodically and assayed at 30 °C using the new fluorometric assay. The residual enzyme activity in the inhibition mixture as compared to the control enzyme activity, obtained in an independent experiment without inhibitor, was plotted over time (Figure 10). The $t_{1/2}$ was collected for each of the examined inhibitor concentrations, and the Kitz and Wilson plot was constructed (Figure 10). The same incubations were repeated at 30 °C with a lower range of inhibitor concentrations (0.125–2 μM). The plots of time dependent loss of enzyme activity and the Kitz and Wilson plot were obtained in a similar manner (Figure S17).

Docking simulation

Docking simulations were conducted with the Accelrys Discovery Studio software package (PC version 1.7). The output docking modes were scored by the newly developed scoring function LigScore2.[25] Only those binding modes where the substrate ammonium group was sufficiently close to the TPQ cofactor and/or Asp385 were considered productive. Ligand structure construction and energy minimization were performed on the Chem3D Pro 10.0 platform of the ChemOffice software package (Cambridge). Only the conjugate acid forms of amine substrates were considered. The most stable all S-trans conformations were constructed, which were then energy optimized by MM2 and saved in MOL format. The crystal structure coordinates of native BPAO (1TU5)[16] in the PDB were loaded on the Discovery Studio software. All the water molecules in the crystal were removed, and hydrogens were added by the program. Since the program cannot add hydrogens correctly to modified residues and also cannot define the charge properties of metal ions correctly, the bond grades and charges of the TPQ cofactor and copper(II) were corrected manually. Protonation states of all other ionizable amino acid residues were set as defined by the program. The active site was then identified, and the energy grid was set automatically by the program. However, the automatically-defined energy grid was too permissive to allow for any productive docking modes in most cases; the ligands would simply be stuck at the mouth rim of the enzyme active site interacting with the

three carboxylic residues Asp179, Asp445 and Glu417. The energy grid was thus contracted appropriately such that at least one productive mode could be defined for each of the substrates examined. To ensure comparability, all ligands were docked into the same energy grid. The energy minimized, most stable ligand structures were loaded. The “energy grid forcefield” was set as “Drieding”. The “conformation search include electrostatic energy” was allowed, the “conformation search number of Monte Carlo trials” was set as 30000, and the “pose saving perform clustering” was allowed, with “pose saving maximum cluster per molecule” being set as 100. Each output pose represents the energy minimum of a cluster of poses, and is thus considered as a docking mode. The “scoring scores” option was set as LigScore2. Other parameters were set as default. After calculation, the output poses were ranked according to the LigScore2 scores, visualized and analyzed. The best scored productive docking modes were identified, and the results are shown in Figure 3, Figure 4, Figure 8, and Figure S1–S10, and Table 1.

Supplementary Material

Refer to Web version on PubMed Central for supplementary material.

Acknowledgment

Financial supports of this work from the National Institutes of Health (GM 48812) and the American Diabetes Association (1-06-RA-117) are gratefully acknowledged. We also thank the laboratory of David M. Dooley, Montana State University, for samples of purified BPAO, AGAO, and PPLO, and the laboratory of Charles L. Hoppel, Case Western Reserve University, for the sample of rat liver mitochondria used in this work.

References and notes

1. Knowles, PF.; Dooley, DM. Metal Ions in Biological Systems. Sigel, H.; Sigel, A., editors. Vol. Vol. 30. New York: Marcel Dekker; 1994. p. 361-403. (b) Klinman JP. Chem. Rev 1996;96:2541–2561. [PubMed: 11848836]
2. For recent reviews, see Yu PH, Wright S, Fan EH, Lun ZR, Gubisne-Harberle D. Biochim. Biophys. Acta 2003;1647:193–199. [PubMed: 12686132] (b) Boomsma F, Bhaggoe UM, van der Houwen AM, van den Meiracker AH. Biochim. Biophys. Acta 2003;1647:48–54. [PubMed: 12686107] (c) O’Sullivan J, Unzeta M, Healy J, O’Sullivan MI, Davey G, Tipton KF. Neurotoxicology 2004;25:303–315. [PubMed: 14697905] (d) Matyus P, Dajka-Halasz B, Foldi A, Haider N, Barlocco D, Magyar K. Curr. Med. Chem 2004;11:1285–1298. [PubMed: 15134520] (e) Boomsma F, Hut H, Bagghoe U, van der Houwen A, van den Meiracker A. Med. Sci. Monit 2005;11:122–126. (f) Obata T. Life Sci 2006;79:417–422. [PubMed: 16487546] (g) Gong B, Boor PJ. Expert Opin. Drug Metab. Toxicol 2006;2:559–571. [PubMed: 16859404] (h) Lucero HA, Kagan HM. Cell Mol. Life Sci 2006;63:2304–2316. [PubMed: 16909208] (i) McDonald IA, Foot J, Yin P, Flening E, van Dam EM. Ann. Rep. Med. Chem 2007;42:229–243. (j) Dunkel P, Gelain A, Barlocco D, Haider N, Gyires K, Sperlagh B, Magyar K, Maccioni E, Fadda A, Matyus P. Curr. Med. Chem 2008;15:1827–1839. [PubMed: 18691041]
3. For a recent review, see Dubois JL, Klinman JP. Arch. Biochem. Biophys 2005;433:255–265. [PubMed: 15581581]
4. (a) Wang SX, Mure M, Medzihradszky KF, Burlingame AL, Brown DE, Dooley DM, Smith AJ, Kagan HM, Klinman JP. Science 1996;273:1078–1084. [PubMed: 8688089] (b) Wang SX, Nakamura N, Mure M, Klinman JP, Sanders-Loehr J. J. Biol. Chem 1997;46:8157–8160.
5. Mure M, Mills SA, Klinman JP. Biochemistry 2002;41:9269–9278. [PubMed: 12135347]
6. Abella A, Marti L, Camps M, Claret M, Fernandez-Alvarez J, Gomis R, Guma A, Viguerie N, Carpene C, Palacin M, Testar X, Zorzano A. Diabetes 2003;52:1004–1013. [PubMed: 12663473]
7. Salter-Cid LM, Wang E, O'Rourke AM, Miller A, Gao H, Huang L, Garcia A, Linnik MD. J. Pharmacol. Exp. Ther 2005;315:553–562. [PubMed: 16081681]
8. (a) Zhang Y, Ran C, Zhou G, Sayre LM. Bioorg. Med. Chem 2007;15:1868–1877. [PubMed: 17150363] (b) Qiao C, Ling KQ, Shepard EM, Dooley DM, Sayre LM. J. Am. Chem. Soc 2006;128:6206–6219. [PubMed: 16669691] (c) Kim J, Zhang Y, Ran C, Sayre LM. Bioorg. Med.

Chem 2006;14:1444–1453. [PubMed: 16266805] (d) Qiao C, Jeon HB, Sayre LM. J. Am. Chem. Soc 2004;126:8038–8045. [PubMed: 15212554]

9. (a) Palamakumbura AH, Trackman PC. Anal. Biochem 2002;300:245–251. [PubMed: 11779117] (b) Matsumoto T, Furuta T, Nimura Y, Suzuki O. Anal. Biochem 1984;138:133–136. [PubMed: 6428269] (c) Trackman PC, Zoski CG, Kagan HM. Anal. Biochem 1981;113:336–342. [PubMed: 6116464]
10. Holt A, Palcic MM. Nat. Protoc 2006;1:2498–2505. [PubMed: 17406497]
11. For recent reviews, see Goddard JP, Reymond JL. Curr. Opin. Biotechnol 2004;15:314–322. [PubMed: 15358001] (b) Goddard JP, Reymond JL. Trends Biotechnol 2004;22:363–370. [PubMed: 15245909] (c) Wahler D, Reymond JL. Curr. Opin. Biotechnol 2001;12:535–544. [PubMed: 11849935]
12. Shepard EM, Smith J, Elmore BO, Kuchar JA, Sayre LM, Dooley DM. Eur. J. Biochem 2002;269:3645–3658. [PubMed: 12153561]
13. Despite the scope of fluorophores being broader following a retro-Michael addition strategy of enzyme visualization, [14] the non-spontaneous nature of the retro-Michael addition (β-elimination) reaction under physiological conditions suggests that fluorogenic substrates of this type would not be able to respond to the enzyme activity in real time.
14. (a) List B, Barbas CF III, Lerner RA. Proc. Natl. Acad. Sci. USA 1998;95:15351–15355. [PubMed: 9860972] (b) Zhou W, Valley MP, Shultz J, Hawkins EM, Bernad L, Good T, Good D, Riss TL, Klaubert DH, Wood KV. J. Am. Chem. Soc 2006;128:3122–3123. [PubMed: 16522074]
15. Kang K-D, Jones PD, Huang H, Zhang R, Mostovich LA, Wheelock CE, Watanabe T, Gulyaeva LF, Hammock BD. Anal. Biochem 2005;344:183–192. [PubMed: 16083846]
16. Lunelli M, Di Paolo ML, Biadene M, Calderone V, Battistutta R, Scarpa M, Rigo A, Zanotti G. J. Mol. Biol 2005;346:991–1004. [PubMed: 15701511]
17. Of the three expected turnover products for compounds **5–7**, only compound **8** was synthesized because its optical properties are significantly different from those of **3** (see Table S1 and Figure S12 in Supporting Information).
18. (a) Di Paolo ML, Stevanato R, Corazza A, Vianello F, Lunelli L, Scarpa M, Rigo A. Biochem. J 2003;371:549–556. [PubMed: 12529179] (b) Di Paolo ML, Scarpa M, Corazza A, Stevanato R, Rigo A. Biophys. J 2002;83:2231–2239. [PubMed: 12324440]
19. Chen, Y.; Sayre, LM. unpublished results
20. In our docking study of these diamine substrates with BPAO, we have also observed major docking modes where the ancillary amino groups were interacting with Glu 417. Thus Glu417 was considered to be a minor contributing residue to the overall substrate binding.
21. (a) Yraola F, Garcia-Vicente S, Fernandez-Recio J, Albericio F, Zorzano A, Marti L, Royo M. J. Med. Chem 2006;49:6197–6208. [PubMed: 17034126] (b) Marti L, Abella A, de la Cruz X, Garcia-Vicente S, Unzeta M, Carpene C, Palacin M, Testar X, Orozco M, Zorzano A. J. Med. Chem 2004;47:4865–4874. [PubMed: 15369390]
22. Bardsley WG, Crabbe MJC, Shindler JS. Biochem. J 1972;127:875–879. [PubMed: 4627688]
23. Hoppel CL, Kerner J, Turkaly P, Turkaly J, Tandler B. J. Biol. Chem 1998;273:23495-235035. [PubMed: 9722587]
24. Janes SM, Klinman JP. Biochemistry 1991;30:4599-460. [PubMed: 2021652]
25. Krammer A, Kirchhoff PD, Jiang X, Venkatachalam CM, Waldman M. J. Mol. Graphics Modell 2005;23:395–407.

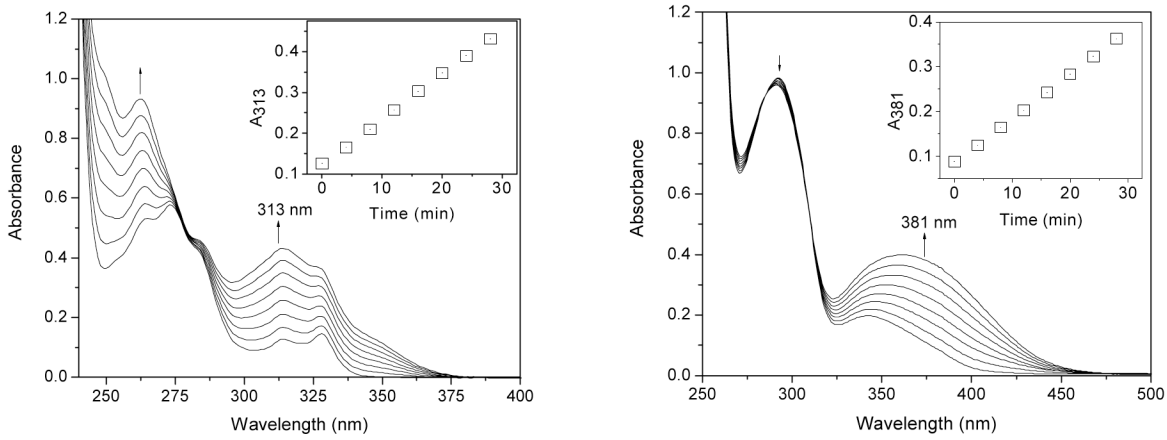

Figure 1.

Time-dependent (4 min interval) UV-vis spectra recorded upon mixing 0.1 mM of **1** (left) or **2** (right) with 0.1 μM of BPAO in 0.1 M of pH 7.2 phosphate buffer at 30 °C. Insets: time dependent plots of absorbance growth at wavelengths indicated.

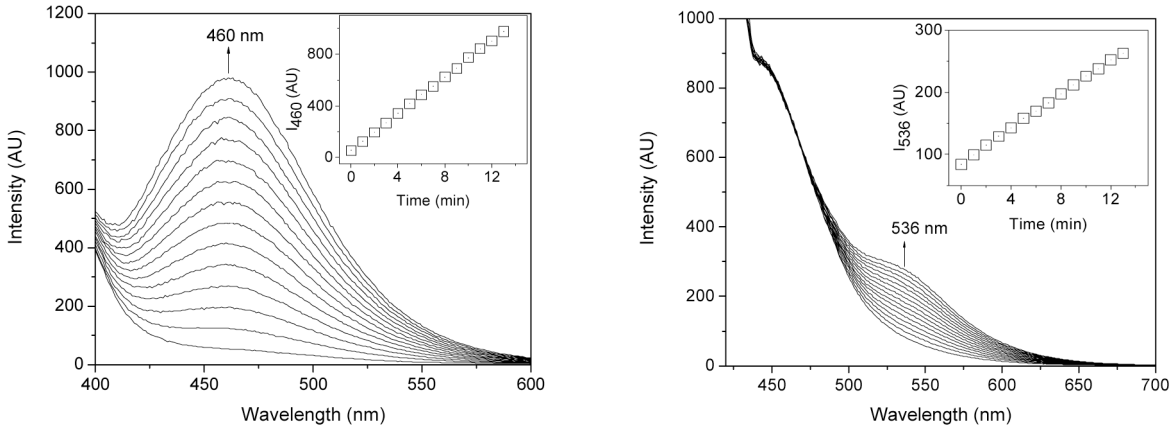

Figure 2.

Time-dependent (1 min interval) fluorescence spectra recorded upon mixing 0.1 mM of **1** (left) or **2** (right) with 5 nM of BPAO in 0.1 M of pH 7.2 phosphate buffer at 30 °C. The λ_{ex} were 350 nm for **1** and 420 nm for **2**. Insets: time-dependent plots of emission growth at wavelengths indicated.

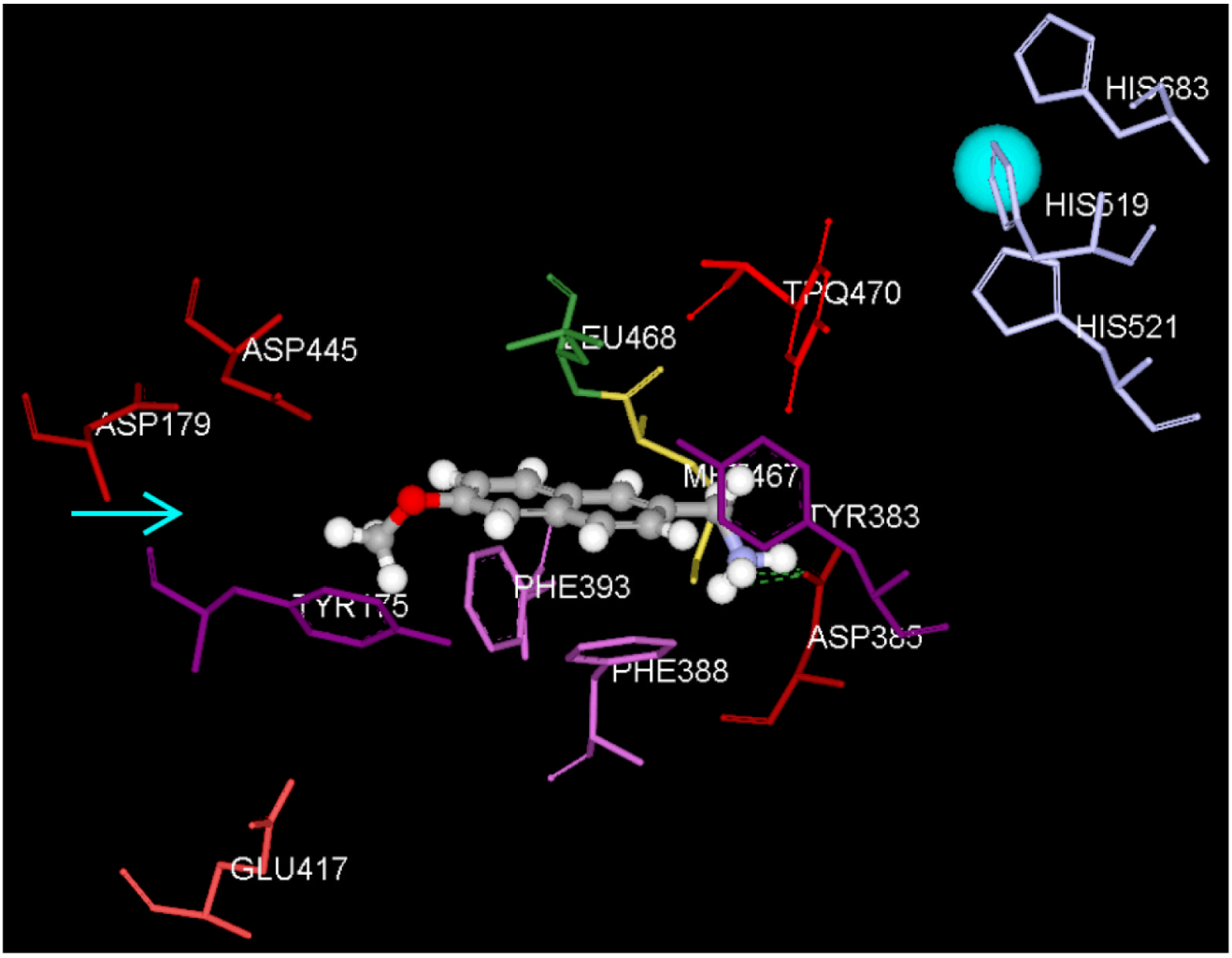

Figure 3.
Docking of **1** into the active site of BPAO. The arrow indicates the mouth opening from where substrate approaches into the active site. The hydrogen bonding between the substrate amino group and Asp385 is noted as green dashed lines.

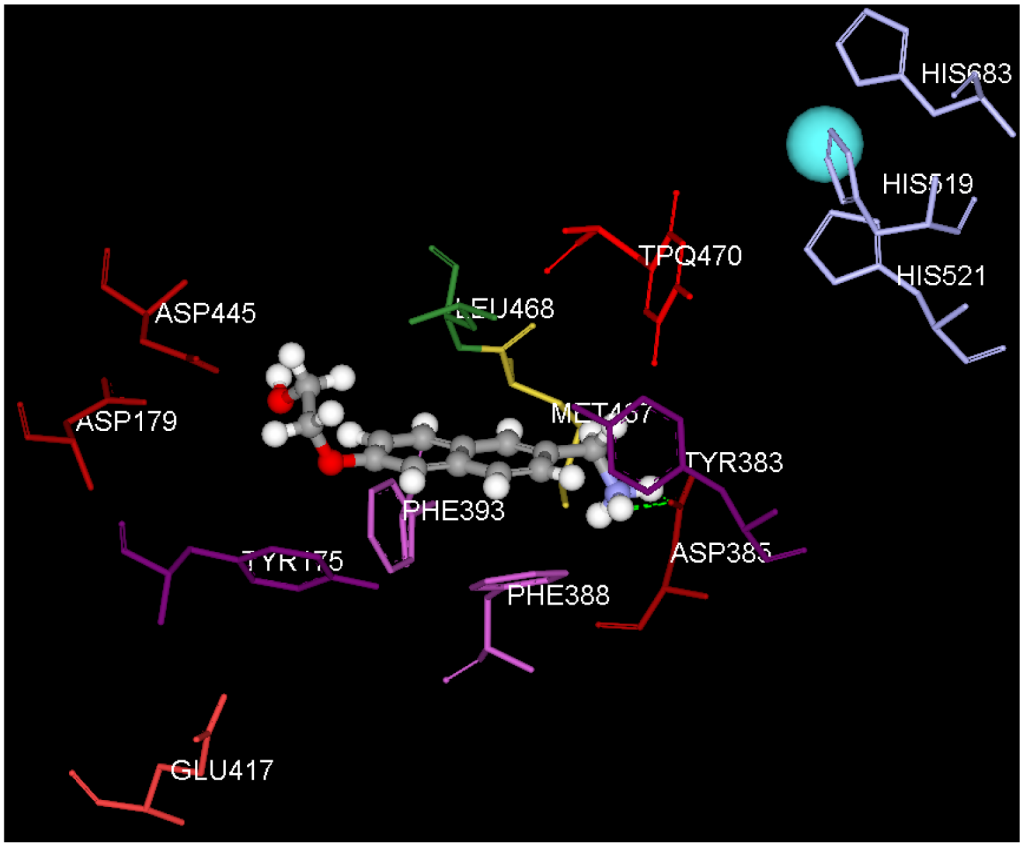

Figure 4.
The best scored productive docking mode of compound **7** with native BPAO. Note that the substrate OH is interacting with Asp445.

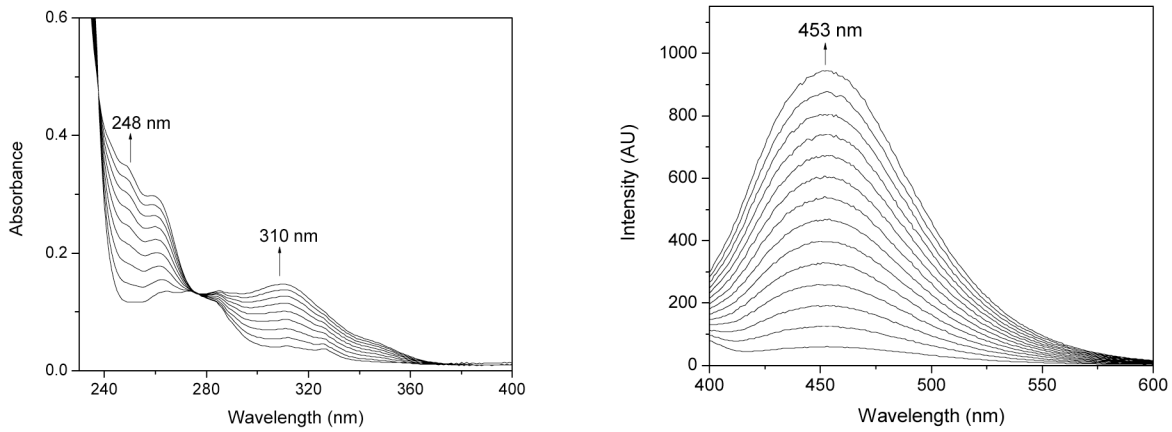

Figure 5.

Left panel: time-dependent (30 s interval) UV-vis spectra recorded upon mixing 20 μM of **12** with 0.1 μM of BPAO in 0.1 M pH 7.2 phosphate buffer at 30 °C. Right panel: time-dependent (1 min interval) fluorescence spectra (λ_{ex} 350 nm) recorded upon mixing **12** (10 μM) with BPAO (1.0 nM) in 0.1 M pH 7.2 phosphate buffer at 30°C.

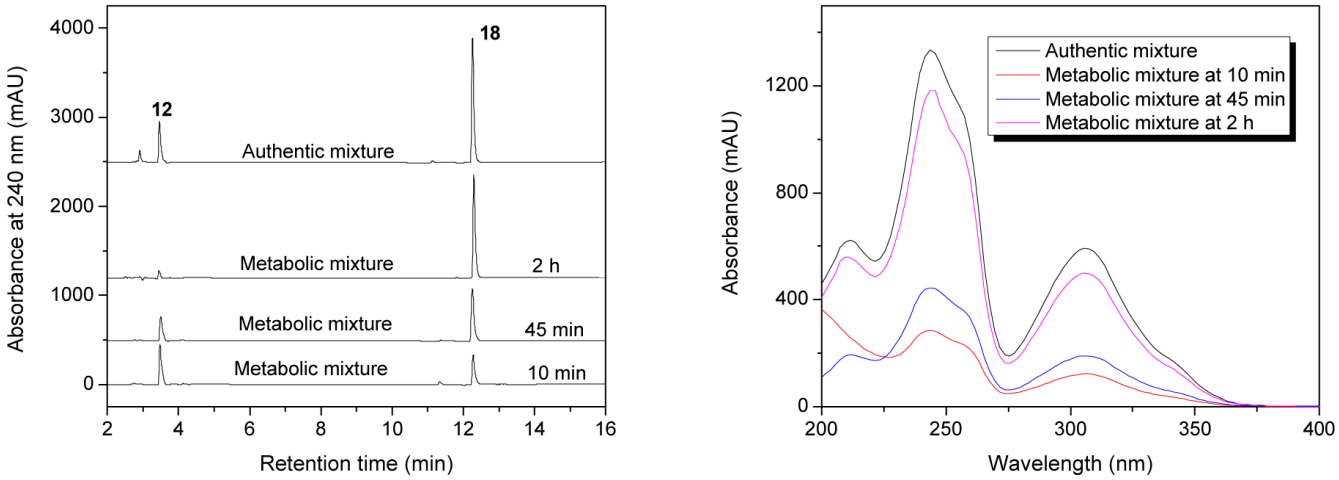

Figure 6.

Left panel: HPLC diagram of a mixture of authentic **12** and **18** (both 200 μM), and time dependent HPLC diagrams of a metabolic mixture of **12** (200 μM) with BPAO (0.1 μM) in 0.1 M of pH 7.2 phosphate buffer at 25 °C. Right panel: the corresponding DAD spectra of peaks at 12.3 min (**18**).

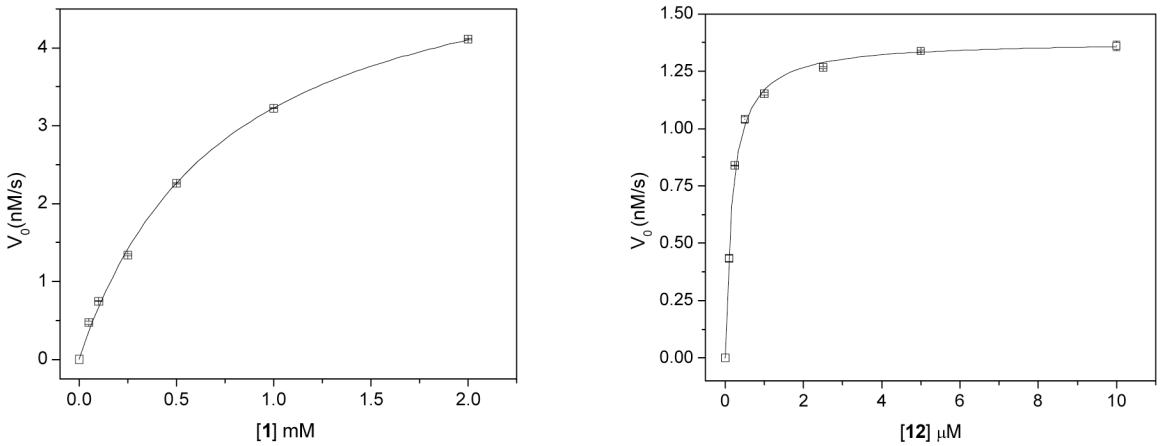

Figure 7.

Plots of initial oxidation velocity (V_0) vs. substrate concentration of **1** in 33 mM of pH 7.2 phosphate buffer in the presence of BPAO (5.0 nM) (left), and of **12** in 0.1 M of pH 7.2 phosphate buffer in the presence of BPAO (2.0 nM) both at 30 °C (right) as measured by fluorescence spectrophotometry.

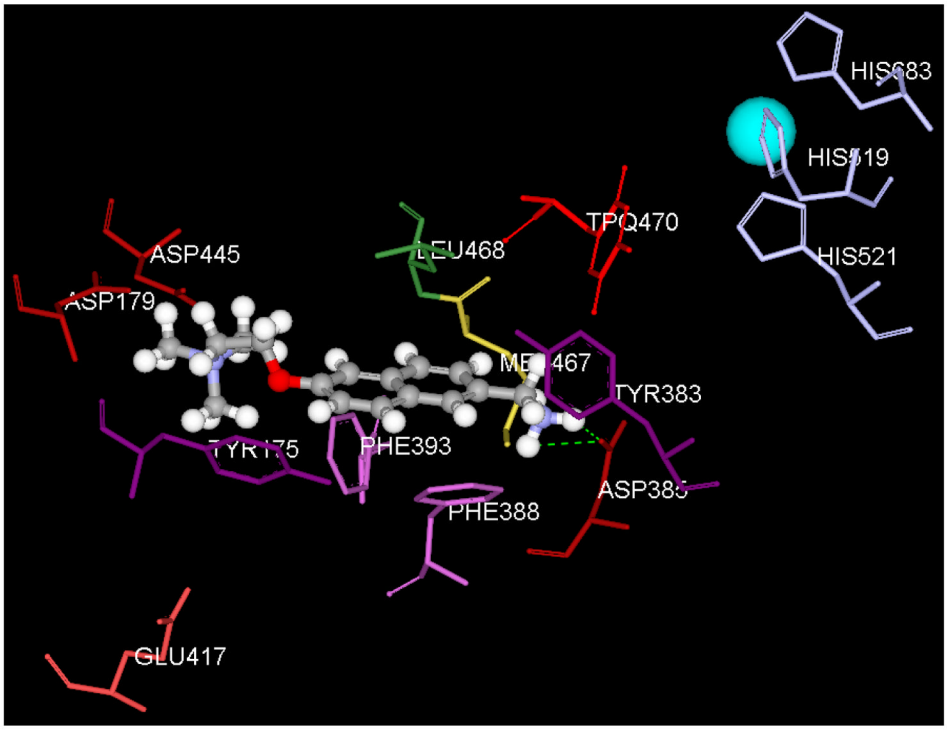

Figure 8.
The best scored productive docking mode of **12** with BPAO. Note that the substrate quaternary ammonium group is close to Asp445 to allow for an additional electrostatic interaction.

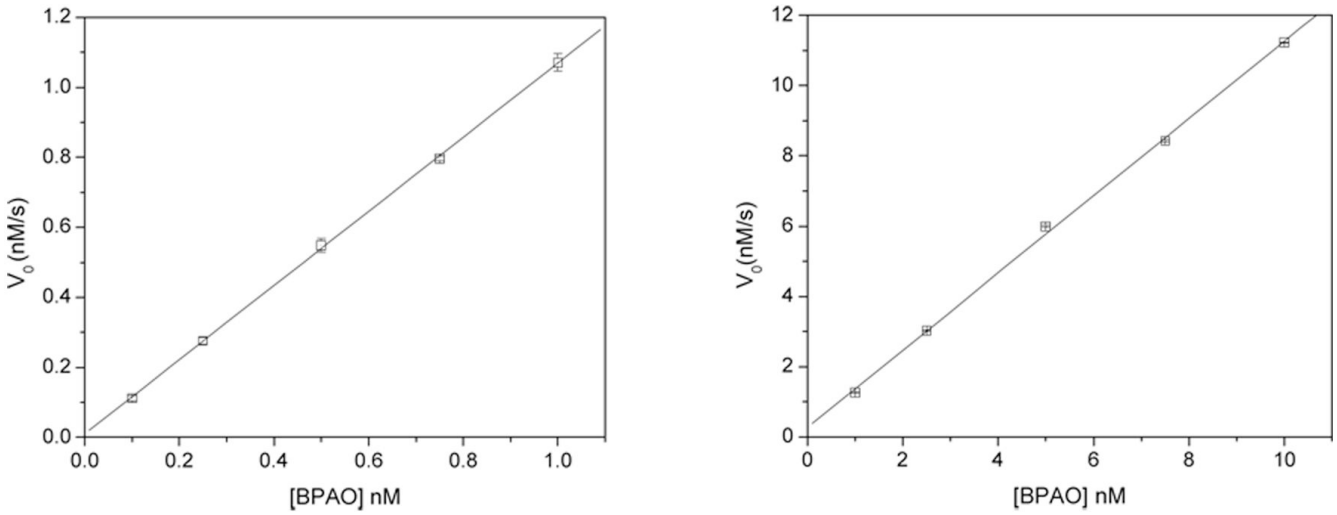

Figure 9.
Linear relationship between enzyme concentration and initial oxidation velocity (V_0) of **12** (10 μM) in 0.1 M of pH 7.2 phosphate buffer at 30 °C. Left: [BPAO] 0–1.00 nM. Right: [BPAO] 1.00–10.0nM.

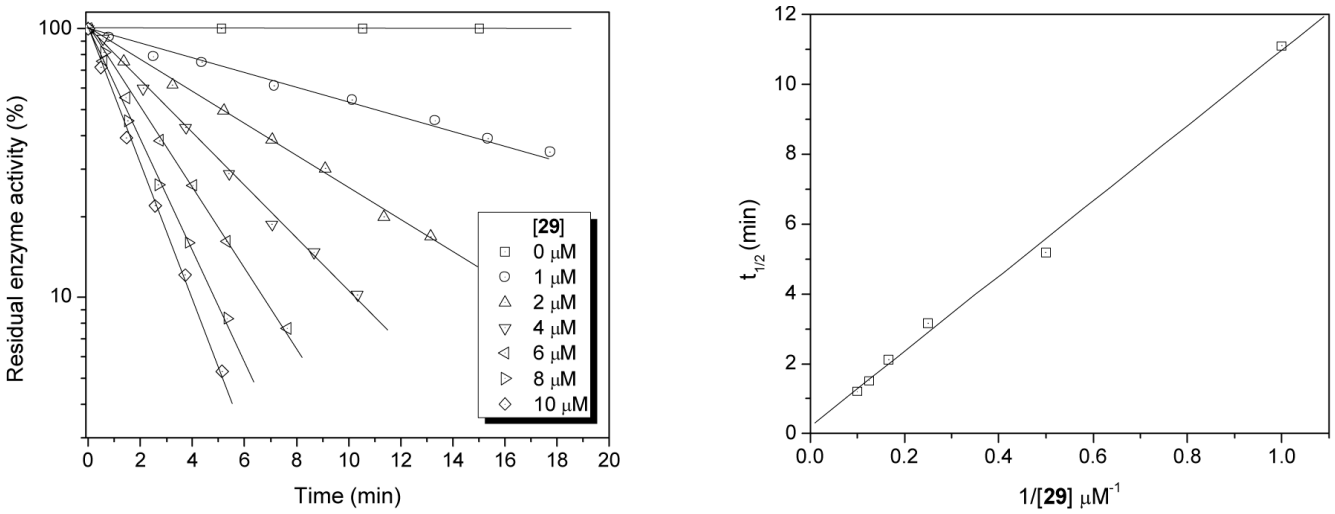

Figure 10.

Time dependent activity loss of BPAO (50 nM) incubated with various concentrations of 1-amino-2,3-butadiene (**29**) in 0.1 M of pH 7.2 phosphate buffer at 2 °C as monitored by the new fluorometric assay (left), and the corresponding Kitz and Wilson plot (right).

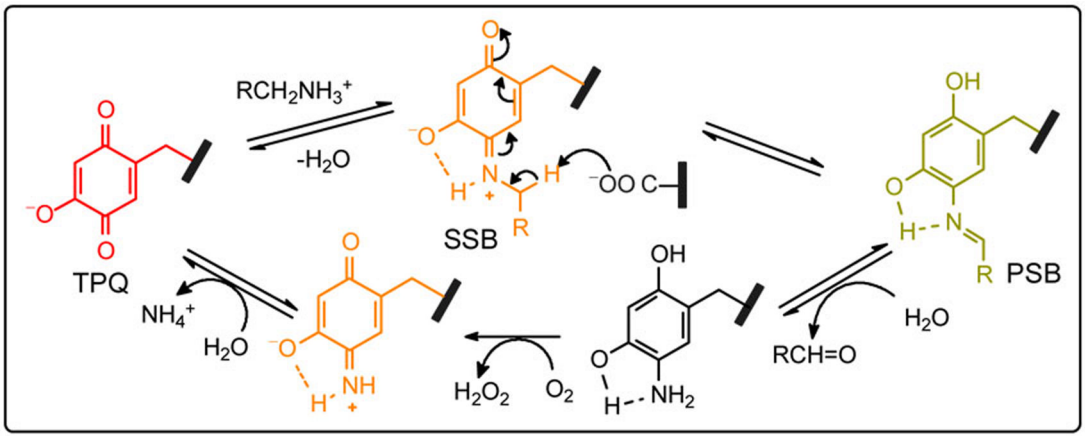

Scheme 1.

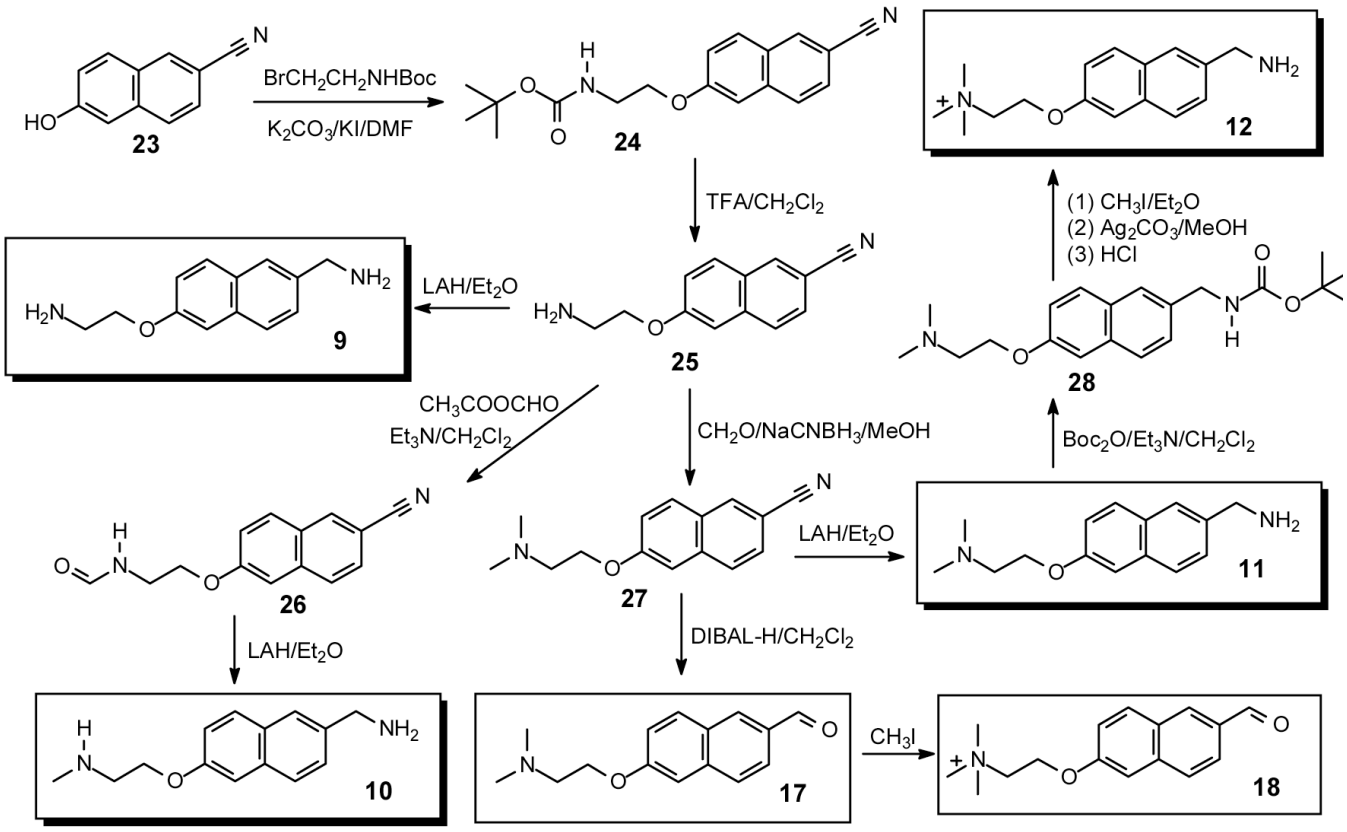

Scheme 2.

Table 1

Computed docking scores of the best scored productive docking modes of arylmethylamines and their experimental substrate activities with BPAO[a]

substrate	docking score[b]	K_m	k_{cat}(s^{-1})	k_{cat}/K_m(M^{-1} s^{-1})	relative activity
BA[c]	0.65	1.77±0.24 mM	1.23±0.06	6.95×10^{2}	1
1[c]	0.39	0.74±0.15 mM	1.15±0.06	1.55×10^{3}	2.2
1		0.74±0.06 mM	1.12±0.04	1.51×10^{3}	2.2
2[c]	0.50	0.10±0.02 mM	0.44±0.02	3.67×10^{3}	5.3
5[c]	0.04	2.92±0.43 mM	1.16±0.08	3.97×10^{2}	5.7×10^{-1}
6[d]	0.49	0.35±0.05 mM	0.256±0.020	7.31×10^{2}	1.1
7[d]	0.64	14.4±5.2 μM	0.034±0.003	2.36×10^{3}	3.4
9[d]	2.16	122±16 nM	0.0244±0.0032	2.00×10^{5}	2.9×10^{2}
10[d]	1.63	209±9 nM	0.212±0.002	1.01×10^{6}	1.5×10^{3}
11	1.94	202±36 nM	0.436±0.020	2.16×10^{6}	3.1×10^{3}
12	2.12	183±14 nM	0.690±0.010	3.77×10^{6}	5.4×10^{3}
13	3.14	163±12 nM	0.302±0.006	1.85×10^{6}	2.7×10^{3}
14	3.42	125±9.6 nM	0.159±0.002	1.27×10^{6}	1.8×10^{3}
15	3.42	78±8.5 nM	0.050±0.001	6.41×10^{5}	9.2×10^{2}
16	3.41	64±15 nM	0.0154±0.0007	2.41×10^{5}	3.5×10^{2}

[a] All the data were measured in pH 7.2 phosphate buffer at 30 °C by fluorescence spectrophotometry unless otherwise stated. Detailed conditions for each reaction are listed in Table S2.

[b] Calculated by Accelrys Discovery Studio using the crystal structure of BPAO from the Protein Data Bank (PDB).

[c] Measured by UV-vis spectrophotometry.

[d] The k_{cat} was estimated using the fluorescence intensity of **3** (for **6**) and of **17** (for **7**, **9**, and **10**); see Supporting Information.

Table 2

Initial oxidation velocities (V_0) for **12** (20 μM) by different amine oxidases as compared to BA or *p*-xylylenediamine (PXDA)[a]

enzyme	V_0 (nM s^{-1})		
	BA[b]	PXDA[c]	12[d]
BPAO	82.8	-	62.3
pkDAO	-	51.8	1.0
AGAO	54.7	-	1.3
PPLO	67.2	-	24.8
MAO-B	103.1	-	0.6

[a] All incubations were conducted in pH 7.2 phosphate buffer and monitored at 250 nm by UV-vis spectrophotometry. Reaction temperatures are 37 °C for pkDAO and 30 °C for all other enzymes.

[b] 5 mM in 50 mM buffer.

[c] 1.5 mM in 0.1 M buffer.

[d] 20 μM in 0.1 M buffer.